ISSN: 0976-9102 (ONLINE)
DOI: 10.21917/ijivp.2021.0354

FRACTIONAL DIFFERENTIATION-BASED EDGE ENERGY DRIVEN ACTIVE CONTOURS FOR ROBUST IMAGE SEGMENTATION

Srikanth Khanna and V. Chandrasekaran
Department of Mathematics and Computer Science, Sri Sathya Sai Institute of Higher Learning, India

Abstract

In this paper, a new fractional differentiation-based active contour model for robust image segmentation is presented. A new edge energy is introduced, in which the contour evolution is driven by the difference between the fractional derivatives directed along the inward and outward normal directions of the evolving contour. We provide the level set formulation of this novel energy and show that this energy is minimized when there is an accurate alignment of the zeroth level set of the evolving contour with the actual object boundary. The proposed model outperforms other state-of-the-art active contour methods in eliciting weak/fuzzy boundaries in real world images and provides robust segmentation even under influence of various types of noise as quantified by segmentation metrics.

Keywords:

Fractional Derivative, Image Segmentation, Active Contour, Edge Energy

1. INTRODUCTION

Image segmentation is an important step in vision tasks as image analysis algorithms greatly depend on the quality of segmentation. Segmentation is the partitioning of an image into non-intersecting regions, where each region is delineated by a predicate that holds true over it and not on adjacent regions. However, in real world images, there is a lot of uncertainty in region/object boundaries. This is due to the natural setting of the image itself, the acquisition process or noise, which make segmentation a challenging task. Segmentation approaches in the literature segregate image regions by formulating a suitable objective functional to identify boundaries and solving the optimization problem arising therefrom.

Active contours employ the numerical formulation of a partial differential equation to achieve image segmentation. To begin with, an initial contour is introduced in the image, which evolves over time. The property that defines the segmentation end result is encoded in the cost functional. The active contour models exploit the information from the image in a variety of ways to define the energy functional.

Kass and Witkin [1] introduced the first energy minimizing curves or snakes, which used a combination of internal and image forces alongside user specified constraints. However, their model had difficulty in handling the topological changes in the contour. Osher and Sethian [2] overcame this drawback by implicitly representing the contour as the zeroth level set of a higher dimensional function.

Edge-based active contour methods like [3]-[6] use peaking in the image intensity variations as the stopping criteria. Edge-based methods are dependent on the initialization and availability of strong gradient information. This dependence on derivative operators makes these methods sensitive to noise and leads to imperfect segmentation in the scenarios where the boundary itself is weak.

Region-based active contours like [7]-[10] use a statistical characterization of each region to evolve the contour. Chan and Vese (CV) [8] proposed a level set implementation of the piece-wise constant approximation of image regions. CV method is demonstrated to be effective on certain cases where edge-based methods are not applicable.

Region-based methods are further classified as methods, which use global information, and those that exploit the local region information. In general, performance of such active contour models is limited by the assumptions that are made about the image regions - like the windows chosen to define image regions under consideration.

Researchers have also adopted hybrid approach, in which the best of both the approaches is being combined successfully for effective active contour evolution. This helps in guiding the contour in the areas where the gradient information is insufficient. Lankton et al. [11] used the mean computed in the interior and exterior neighborhoods around each point along the evolving contour as a hybridization of the geodesic and region-based methods. Kim et al. [13] employed a new higher order statistics-based edge energy to be used alongside the local region energy in the variational formulation to segment only the important local minima. In [6], external energy is coupled with a distance regularization term which eliminates the need for reinitialization. In [18], an "importance" parameter is computed based on the local edge features, which is used to weight the energy terms in the evolution equation.

Our active contour model recognizes edge as a transition boundary between two regions. The long memory property of fractional derivatives, which allows them to "see" further than their integer order counterparts, is harnessed. In our method, therefore, the intensity variation among pixels is considered but alongside a reasonable amount of region information too is brought into consideration due to the use of fractional derivatives. This gives a broader evidence of region boundaries compared to the other state-of-the-art methods, and helps extract boundaries unavailable to standard edge-based methods.

2. MATHEMATICAL BACKGROUND

2.1 FRACTIONAL DIFFERENTIATION

Fractional calculus is an extension of traditional calculus that has its origins in the question by Liouville. Several great mathematicians have hence worked on this topic and even to this date, the definition of fractional derivative is an active field of research [19], [20]. Fractional derivatives are interpolations of integer order derivatives and are recognized in the recent years for their ability to model long memory processes and are shown to be

robust against noise. One-sided fractional derivatives are a 1D implementation of the fractional derivative definition, and have gained prominence in signal processing along with their multi-directional combinations [21]-[25]. We use the Grunwald-Letnikov (G-L) definition for our numerical calculations owing to computational convenience, and we use its truncated series representation for our digital image processing computations. In this section, we provide the definitions of the fractional order derivatives, which will be used in the subsequent sections.

Let $f(t)$ be a signal to be analyzed in a finite interval $[a,b]$. $D_{a^+}^{\alpha}$ and $D_{b^-}^{\alpha}$, the "left" and "right" one-sided G-L derivatives of order α, $0<\alpha<1$, are given by:

$$D_{a^+}^{\alpha} f(t) = \lim_{h\to 0} h^{-\alpha} \sum_{j=0}^{N_1} (-1)^j \binom{\alpha}{j} f(t-jh) \tag{1}$$

where $t=a+N_1h$ and

$$D_{b^-}^{\alpha} f(t) = \lim_{h\to 0} h^{-\alpha} \sum_{j=0}^{N_2} (-1)^j \binom{\alpha}{j} f(t+jh) \tag{2}$$

where $b=t+N_2h$.

2.2 ACTIVE CONTOUR METHODS

In active contour literature, a Lipschitz function ϕ: $\Omega\to\mathbb{R}$ denotes the level set function and $\{\phi(x,y)=0, (x,y)\in\Omega\}$, the zeroth level set, is used to track the evolving contour.

We use the definition

$$H_\varepsilon(\phi) = \frac{1}{2} + \frac{1}{\pi}\arctan\left(\frac{\phi}{\varepsilon}\right) \tag{3}$$

From [8], to denote the Heaviside function. $H_\varepsilon(\phi)$ denotes the interior of the contour and its derivative δ_ε, the Dirac delta function, defined as

$$\delta_\varepsilon(\phi) = \frac{\varepsilon}{\pi\left(\phi^2+\varepsilon^2\right)} \tag{4}$$

The Eq.(4) denotes the immediate area around the contour. Here the parameter ε controls the smear of the Dirac function.

The gradient flow of the Distance Regularized Level Set Evolution (DRLSE) method [6] is given as:

$$\frac{\partial\phi}{\partial t} = \mu\nabla\cdot\left(d_p\left(|\nabla\phi|\right)\nabla\phi\right) - \frac{\partial E_{ext}}{\partial\phi} \tag{5}$$

where $\mu d_p(|\nabla\varphi|)$ is the adaptive forward-and-backward diffusion rate, which is responsible for maintaining the signed distance property.

As mentioned in the introduction, there are active contour methods which take into consideration the region information around the edges. We now discuss the related state-of-the-art in such active contour models.

The localized region-based active contour (LAC) proposed by Lankton et al. [11], [12] is given as:

$$\frac{\partial\phi}{\partial t} = \delta\phi(x)\int_{\Omega_y} B(x,y)\delta\phi(y)\cdot \left(I(y)-u_x\right)^2 - \left(I(y)-v_x\right)^2 dy + \lambda\delta\phi(x)\kappa \tag{6}$$

where $\kappa = \nabla\cdot\dfrac{\nabla\phi}{|\nabla\phi|}$.

This flow localizes the uniform modeling energy by [8], which reaches its stable minimum when the local interior and local exterior in the neighborhood $B(x,y)$ about each point along the contour are modeled by the interior and exterior means.

The region scalable fitting energy (RSF) proposed by Li et al. [26] is given by the gradient flow:

$$\frac{\partial\phi}{\partial t} = -\delta_\varepsilon(\phi)\left(\lambda_1 e_1 - \lambda_2 e_2\right) + \nu\delta_\varepsilon(\phi)\kappa + \mu\left(\nabla^2\phi - \kappa\right) \tag{7}$$

Here, the first term on the right is the data fitting term, which brings into consideration the local approximation of energies on both sides of the evolving contour.

Energies with fractional derivative based piecewise constant Mumford-Shah fitting terms have been proposed in [14]-[17]. In [15], the fitting energy is constructed based on the difference image obtained by subtracting the fractional order gradient magnitude from the original image.

3. PROPOSED MODEL

There are several methods that utilize the concept of edge to arrive at a segmentation of the object. Firstly, all such methods are sensitive to initialization since such models seek out the nearest edge. Secondly, the presence of even small quantities of noise would upset their segmentation performance since edge-based methods rely on the discriminating power of the first or second order derivatives. In this paper, we propose a novel edge-based method which overcomes the second challenge. In scenarios with simple initializations, we demonstrate that using the fractional order derivatives to conceptualize the object boundary, the proposed edge-based method is able perform on par with the state-of-the-art region-based and hybrid active contour models in the presence of high noise!

3.1 FRACTIONAL DIFFERENTIATION BASED EDGE ENERGY DEFINITION

Noise resilience of the difference of 1-D fractional derivative operators has been discussed in [21], [24]. Due to this desirable property, our method employs the one-sided fractional derivatives to capture additional region information near the edge. Each such 1-D fractional derivative centered on the evolving contour and acting on the pixels in the neighborhood region captures the intensity profile information in that direction. If we consider only the immediate change in intensity right at the boundary, the formulation becomes extremely sensitive to noise. A fractional derivative on the contour gives the support of region information alongside the derivative-based intensity variation. Also, the presence of a non-local derivative brings in sensitivity to the objects in a distance.

From the concept of "directional snake" introduced by Park et al. [27], many authors [28]-[30] considered the alignment with the image gradient helpful in evolving the level sets in the right direction in the presence of noise. Motivated by this, in each iteration, we compute the one-sided fractional derivatives in the image $I(x,y)$ along the inward and outward normal directions of the evolving contour. That is, once an initial contour is introduced,

the level set formulation is employed to compute the normal to the curve, and this in turn is used to compute the fractional derivatives in both the normal directions.

Let $\theta(x,y)$ be the gradient direction of the contour $\phi(x,y)$ at a location (x,y). One-sided fractional derivative definitions in and opposing this direction are given as:

$$D_{\theta}^{\alpha} I(x,y) = h^{-\alpha} \sum_{j=0}^{N_1} (-1)^j \binom{\alpha}{j} I(x+\tau_1, y+\tau_2) \tag{8}$$

and

$$D_{\theta+180}^{\alpha} I(x,y) = h^{-\alpha} \sum_{j=0}^{N_2} (-1)^j \binom{\alpha}{j} I(x-\tau_1, y-\tau_2) \tag{9}$$

where $\tau_1 = jh\cos\theta$ and $\tau_2 = jh\sin\theta$.

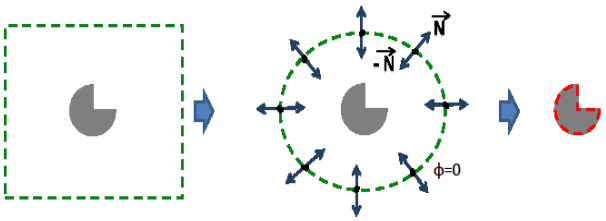

Fig.1. Fractional derivative along the normal directions of the zeroth contour

Their difference, then, is used to drive the contour evolution in the energy minimization iterations. With the appropriate choice of parameters, the contour starts to align with the actual boundary of the object. The contour evolution process halts when the alignment is complete as shown in Fig.1. Thus, our model employs the difference of non-local fractional derivatives across the contour in the normal directions to detect the edges accurately, which is a unique hybrid active contour constitution.

3.2 LEVEL SET FORMULATION OF THE PROPOSED MODEL

We use level set method to track the evolving contour wherein the energy is formulated as follows:

$$E(\phi) = \int_{\Omega} g\delta(\phi)|\nabla\phi| \tag{10}$$

where

$$g(x,y) = -\left(\lambda_1 D_{\theta}^{\alpha} - \lambda_1 D_{\theta+180}^{\beta}\right) \tag{11}$$

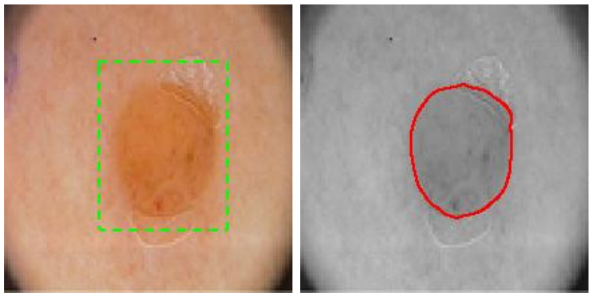

(a) (b)

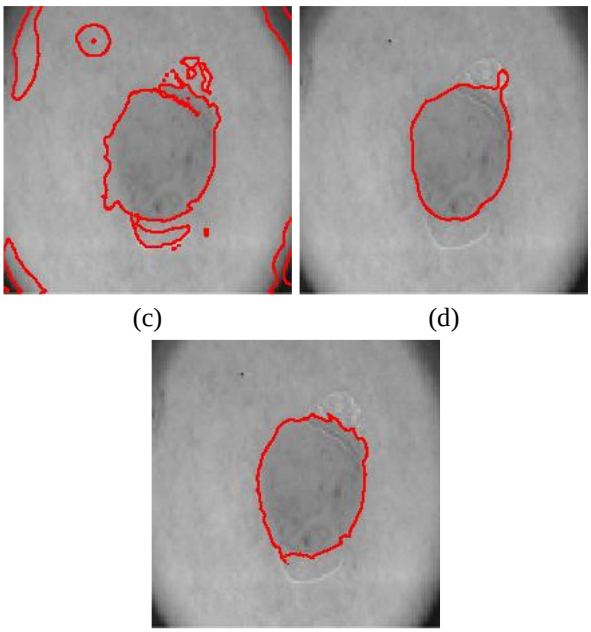

(c) (d)

(e)

Fig.2. (a) Original (b) Proposed (c) RSF (d) DRLSE (e) LAC

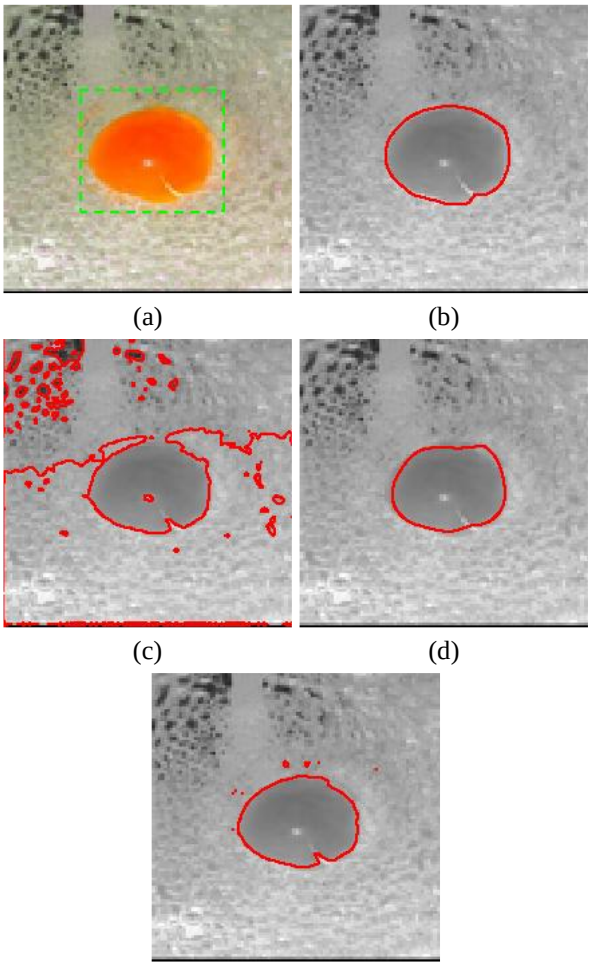

(a) (b)

(c) (d)

(e)

Fig.3. (a) Original (b) Proposed (c) RSF (d) DRLSE (e) LAC

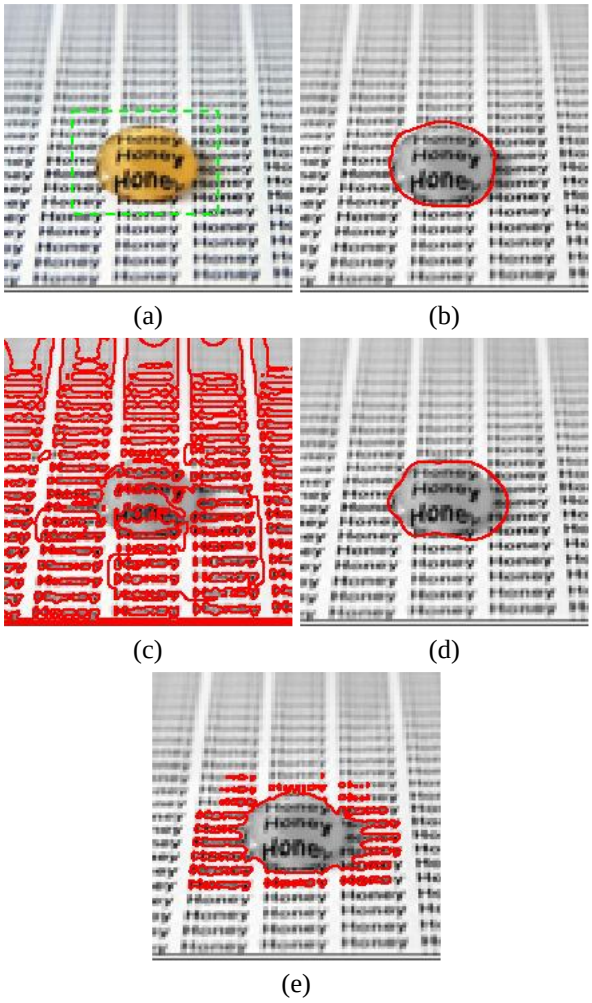

(a) (b) (c) (d) (e)

Fig.4. (a) Original (b) Proposed (c) RSF (d) DRLSE (e) LAC

Table.1. Segmentation Accuracy

Figure	Dice	Jaccard	BF1	Precision	Recall
Fig.2					
Proposed Fig.2(b)	**96.48**	**93.21**	**85.71**	**84.55**	**86.92**
RSF Fig.2(c)	67.33	50.76	23.02	14.1	62.62
DRLSE Fig.2(d)	95.14	90.73	80.86	75.59	86.92
LAC Fig.2(e)	91.52	84.36	45.54	41.48	50.47
Fig.3					
Proposed Fig.3(b)	**96.42**	**93.09**	**96.12**	**96.15**	**96.08**
RSF Fig.3(c)	31.33	18.57	13.83	7.52	85.29
DRLSE Fig.3(d)	92.78	86.53	57.89	58.95	56.86
LAC Fig.3(e)	95.12	90.69	75.57	69.83	82.35
Fig.4					
Proposed Fig.4(b)	**94.45**	**89.48**	**83.98**	**83.52**	83.44
RSF Fig.4(c)	12.45	6.64	5.65	2.91	**95.56**
DRLSE Fig.4(d)	90.01	81.84	64.84	64.13	65.56
LAC Fig.4(e)	70.62	54.59	24.43	14.31	83.33

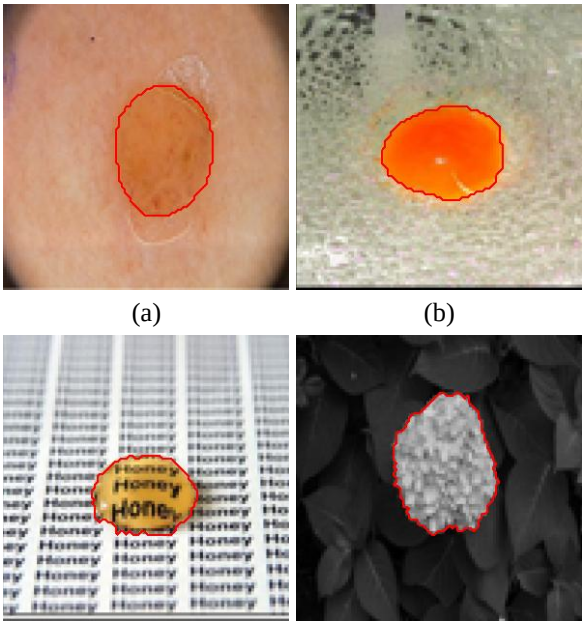

(a) (b) (c) (d)

Fig.5. Segmentation ground truths (a) Fig.2 (b) Fig.3 (c) Fig.4 (d) Fig.6-Fig.9

As in [3], the energy described here seeks segmentation of objects using a new definition of length. Weighting the Euclidean length element by g and considering the line integral, seeks out the object boundaries in the image.

We employ artificial time to obtain a dynamic system. The gradient descent flow evolution equation obtained for the energy functional Eq.(10) is given as:

$$\frac{\partial \phi}{\partial t} = \left(\nabla \cdot \left(\delta g_{\phi_x}, \delta g_{\phi_y}\right) - g\delta_\phi\right)\left|\nabla\phi\right| + \left(g_{\phi_x}, g_{\phi_y}\right)\cdot\nabla\left(\left|\nabla\phi\right|\right) + \nabla\left(g\delta\right)\cdot\vec{N} + gk \quad (12)$$

with the initial condition $\phi(x,y,0) = \phi_0(x,y)$ on Ω. Here,

$$\vec{N} = \frac{\nabla\phi}{\left|\nabla\phi\right|}.$$

Weighting with g directs the balloon term $g\delta_\phi\left|\nabla\phi\right|$ towards objects. Analogous to the discussion for the geodesic problem in [3], $\nabla\left(g\delta\right)\cdot\vec{N}$ term leads the evolving contour into the valley of g and $g\kappa$ term decreases the total curvature. $\left(g_{\phi_x}, g_{\phi_y}\right).\nabla\left(\left|\nabla\phi\right|\right)$ functions like the surface diffusion term discussed in [31].

$\nabla\cdot\left(\delta g_{\phi_x},\delta g_{\phi_y}\right)\left(|\nabla\phi|\right)$ is the area term. Our model does not need any re-initialization.

We discretize the time dependent level set function in Eq.(12) using the techniques discussed in [32], [33]. Stability is achieved using an explicit total variation diminishing third-order Runge-Kutta time discretization with the CFL constant 1.

Let ϕ^n denote the level set solution obtained in the n^{th} iteration, L denote the finite difference approximation of the right-hand side of Eq.(12) and Δt denote the quantum of time stepping. The third-order total variation diminishing optimal Runge-Kutta method solution for the model in Eq.(12) is given as:

$$\begin{aligned} T^{(1)} &= \phi^n + \Delta t L\left(\phi^n\right) \\ T^{(2)} &= \frac{3}{4}\phi^n + \frac{1}{4}T^{(1)} + \frac{1}{4}\Delta t L\left(T^{(1)}\right) \\ \phi^{n+1} &= \frac{1}{3}\phi^n + \frac{2}{3}T^{(2)} + \frac{2}{3}\Delta t L\left(T^{(2)}\right) \end{aligned} \tag{13}$$

In a clutter of objects, shorter memory length may be employed in the fractional derivative definition to avoid influence of neighboring objects at the same time retaining the nonlocal nature of the operators. The value of $h(x,y)$ in the fractional derivative definition depends on the angle $\theta(x,y)$ – it is one-pixel unit in horizontal and vertical directions and $\sqrt{2}$ pixel units in any of the diagonal directions.

3.3 SEGMENTATION EVALUATION

We use Sorenson-Dice and Jaccard similarities to compare the segmented region to that in the ground truth. If P and G denote the prediction and the ground truth respectively, and $|X|$ denotes the cardinality of the set X, the Sorenson-Dice similarity is given by:

$$dice\left(P,G\right) = \frac{2*|P\cap G|}{|P|+|G|}$$

Similarly, the Jaccard dissimilarity coefficient is given by

$$jaccard\left(P,G\right) = \frac{|P\cap G|}{|P\cup G|} = \frac{|P\cap G|}{|P|+|G|-|P\cap G|}$$

In our case, the prediction P is obtained from the final convergence level set solution as $\phi^{final} > 0$ which represents the predicted inside part of the object region. The ground truth G is obtained from the image datasets [35]-[37].

Also since proposed method is an edge-based method, the boundary precision is also computed and tabulated. This is done using the concepts of precision, recall and boundary F1 measure. Precision of the predicted segmentation is the ratio of the number of correctly predicted boundary points with that of the total number of predicted boundary points. Recall is the ratio of the number of ground truth boundary points that are close to the predicted boundary versus the total length of the ground truth boundary. The F1 score of the boundary is a statistical measure computed as follows:

$$BF1\left(P,G\right) = \frac{2*Precision\left(P,G\right)*Recall\left(P,G\right)}{Precision\left(P,G\right)+Recall\left(P,G\right)}$$

We use the MATLAB functions *dice*(*P*,*G*) and *jaccard*(*P*,*G*) and *bfscore*(*P*,*G*). Since the images taken are challenging in terms of the weak boundaries, difficult backgrounds and high noise, the tolerance value which decides the closeness of the predicted and ground truth boundaries is set at 2 pixels for all the methods.

All the above region and boundary precision indices give the segmentation accuracy evaluation in the range [0,1]. These values are multiplied by 100 to provide a percentage value of achieved segmentation accuracy and given in Table.1 and Table.2.

4. EXPERIMENTAL RESULTS AND DISCUSSION

Now we demonstrate the boundary eliciting capability of the proposed method. We compare our results with the state-of-the-art methods: RSF [26], DRLSE [6] and LAC [11]. RSF is a successful region-based method which uses a localizing kernel function in the fitting term to achieve good segmentation. DRLSE uses an edge-based term in distance regularized level set framework. LAC model utilizes the local statistics to evolve the zeroth level set. Uniformly in every row of images, first column shows the test image with initialization marked, the second to fifth columns show the results of the proposed method, RSF, DRLSE and LAC methods respectively.

The default parameters used for each of the methods are mentioned here.

For RSF, Δt=0.1, λ_1=λ_2=1, ν=30, μ=1 and the scale parameter used for Gaussian kernel was 10.

For DRLSE, Δt=1 and coefficient of area term α=-3.

For LAC, λ=0.05 and radius=15 pixels.

For the proposed algorithm, Δt=0.1.

The experiment-specific parameters are mentioned immediately after the corresponding discussion.

We use a simple rectangle signed distance function initialization in all the experiments. The model convergence of the proposed algorithm is on the lines of [34]. We test our algorithm on challenging images from [35]-[37]. Segmentation ground truth boundaries for the various test images are shown in Fig.5.

These results are tabulated in Table 1 for Fig.2-Fig.4 and in Table.2 for Fig.6-Fig.9. Each row in the table records the results for a particular method in terms of region and boundary segmentation accuracy metrics for a particular figure.

In our first experiment, we test the efficacy of our algorithm on a skin lesion image in Fig.2. A good part of the lesion boundary is hazy and has non-uniform illumination across the boundary. As can be seen from the experimental results, our algorithm is able to find the object boundary close to the ground truth even when there is no edge present.

Proposed: α=0.54, β=0.81, λ_1=3, λ_2=3.

RSF: σ=1.

DRLSE: μ=0.08 and Gaussian kernel scale parameter σ=1.

In our next experiment, the proposed active contour algorithm successfully encircles the object in the images with heavy background clutter. As can be seen from Fig.3, the background distractors adversely affect the working of many algorithms but the proposed method gives a steady segmentation result.

Proposed: α=0.36, β=0.81, λ_1=3, λ_2=3.

RSF: σ=10.

DRLSE: μ=0.06, σ=2.

In test on Fig.4, we demonstrate the working of our algorithm on the image of a honey drop on a printed paper. The honey drop boundaries are vague and also the presence of text complicates the segmentation task. Most of the other methods are able to approach the boundary but our method outperforms others with a clear segmentation.

Proposed: α=0.23, β=0.81, λ_1=1, λ_2=1.

RSF: σ=1.

DRLSE: μ=0.06, σ=3.

Next we test our algorithm on the textured image of a flower in the background of leaves in Fig.6. Our algorithm is able to detect the object boundaries comparable to the state-of-the-art.

Proposed: α=0.63, β=0.81, λ_1=-5, λ_2=-5.

RSF: σ=10.

DRLSE: μ=0.04, σ=2.

We now demonstrate the effect of adding varieties of noise to Fig.5. The parameters of the proposed method are left unchanged showcasing the fact that proposed method's parameters are stable even in presence of high noise of different types!

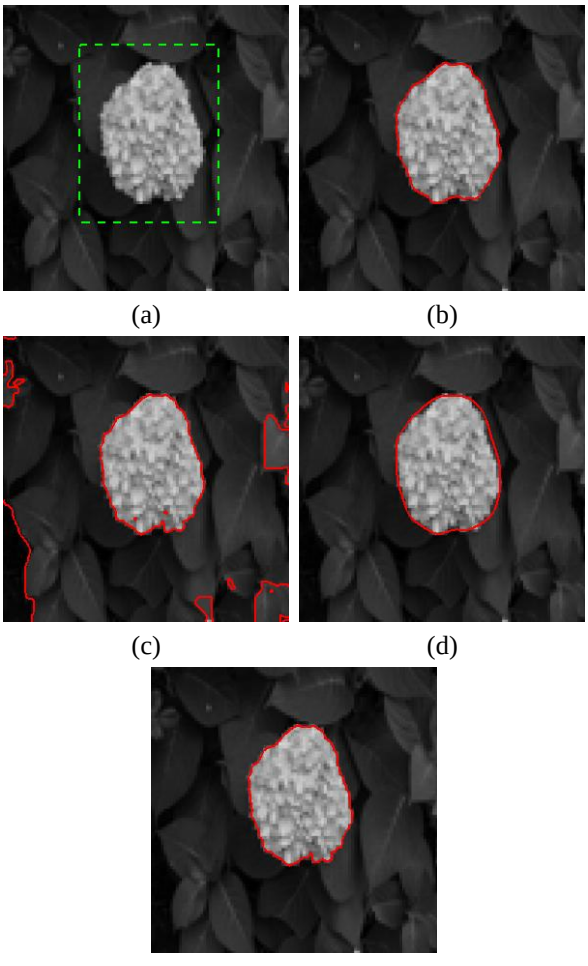

Fig.6. (a) Original (b) Proposed (c) RSF (d) DRLSE (e) LAC

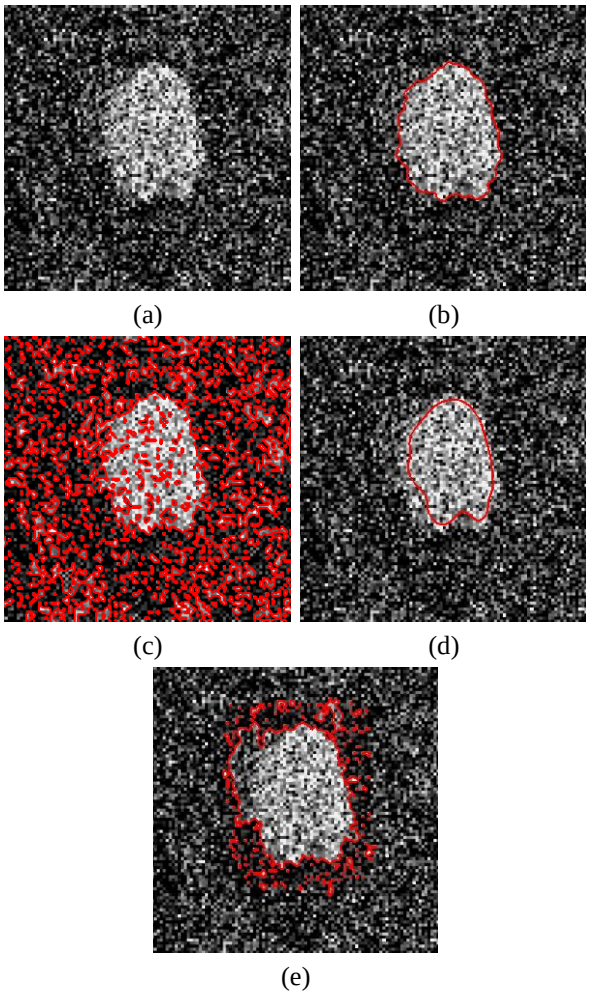

Fig.7. (a) Original (b) Proposed (c) RSF (d) DRLSE (e) LAC

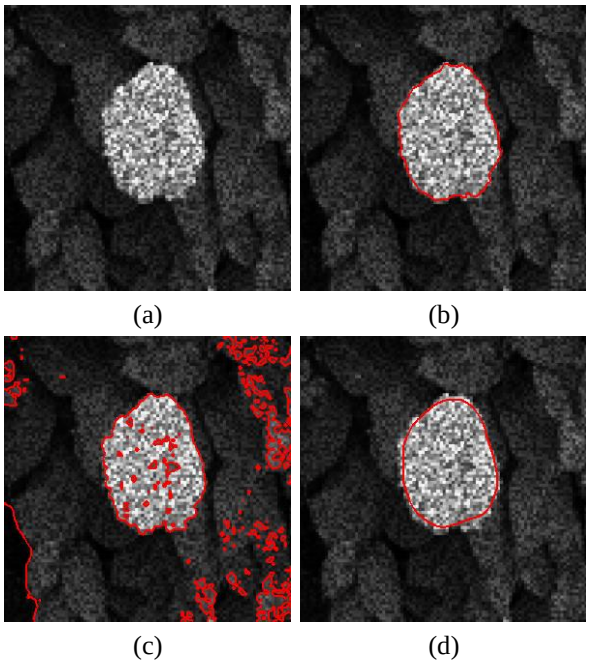

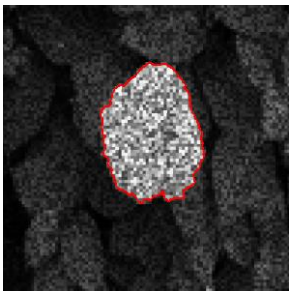

(e)

Fig.8. (a) Original (b) Proposed (c) RSF (d) DRLSE (e) LAC

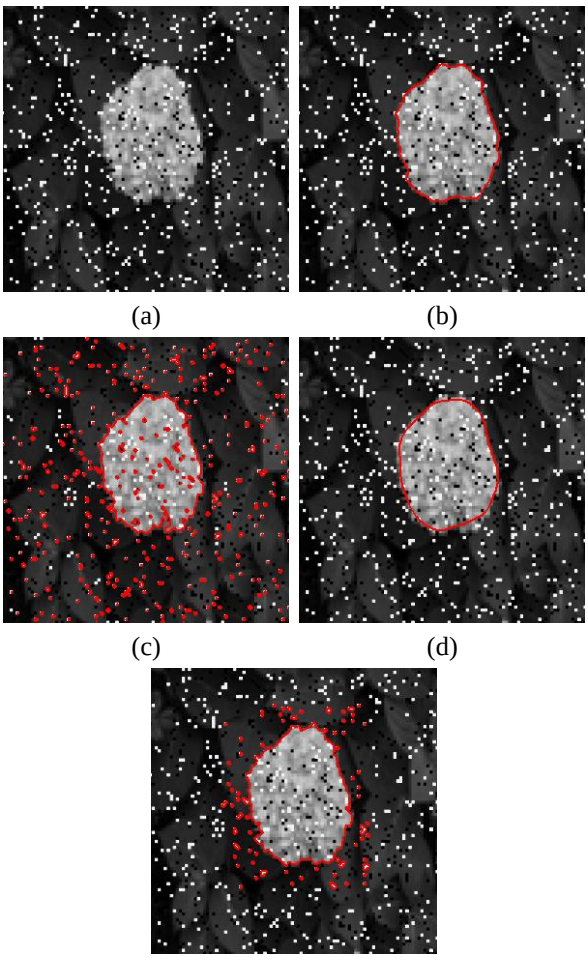

(a) (b)

(c) (d)

(e)

Fig.9. (a) Original (b) Proposed (c) RSF (d) DRLSE (e) LAC

Firstly, we add white Gaussian noise with 0.1 variance to the image. As can be seen from Fig.7, the image is garbled and the boundaries are barely visible.

RSF: σ=10.

DRLSE: μ=0.02, σ=2.5.

We then apply multiplicative speckle noise of 0.1 variance as seen in Fig.8.

RSF: σ=10.

DRLSE: μ=0.01, σ=2.25.

We also test the proposed algorithm by adding salt and pepper noise of density 0.1 to the test image as seen in Fig.9.

RSF: σ=10.

DRLSE: μ=0.08, σ=2, α=-7.

Table.2. Segmentation Accuracy

Figure	Dice	Jaccard	BF1	Precision	Recall
Fig.6					
Proposed Fig.6(b)	98.29	96.63	**100**	**100**	**100**
RSF Fig.6(c)	70.7	54.67	38.91	24.15	100
DRLSE Fig.6(d)	96.44	93.12	89.56	91.38	87.8
LAC Fig.6(e)	**98.6**	**97.24**	98.77	97.56	100
Fig.7					
Proposed Fig.7(b)	**96.26**	**92.79**	**91.73**	**91.6**	91.87
RSF Fig.7(c)	41.1	25.87	10.34	5.46	**96.75**
DRLSE Fig.7(d)	84.23	72.76	22.8	24.75	21.14
LAC Fig.7(e)	79.41	65.85	33.25	21.73	70.73
Fig.8					
Proposed Fig.8(b)	97.22	94.59	**96.24**	**96.55**	95.93
RSF Fig.8(c)	63.87	46.92	21.47	12.08	96.75
DRLSE Fig.8(d)	92.43	85.92	56.2	60	52.85
LAC Fig.8(e)	**97.7**	**95.5**	94.41	92.19	**96.75**
Fig.9					
Proposed Fig.9(b)	**97.52**	**95.15**	**97.51**	**98.28**	96.75
RSF Fig.9(c)	81.18	68.32	31.49	18.8	96.75
DRLSE Fig.9(d)	94.92	90.33	78.86	82.41	75.61
LAC Fig.9(e)	94.81	90.14	73.99	58.72	**100**

The Fig.7 - Fig.9 demonstrate the efficacy of the proposed method in terms of highly accurate and robust segmentation in presence of noise operating under the same parameters chosen for the no-noise scenario as in Fig.6(b).

5. CONCLUSION

Contrary to the belief that edge-based models for object segmentation are poor performers in noisy environment, we have

demonstrated that fractional order derivative-based edge energy driven active contour is robust and outperforms the state-of-the-art techniques. Our future work will delve into predicting optimal fractional order, speeding up the evolution computations vis-a-vis a variety of initializations.

REFERENCES

[1] M. Kass, A. Witkin and D. Terzopoulos, "Snakes: Active Contour Models", *International Journal of Computer Vision*, Vol. 1, No. 4, pp. 321-331, 1988.

[2] S. Osher and J.A. Sethian, "Fronts Propagating with Curvature-Dependent Speed: Algorithms based on Hamilton-Jacobi Formulations", *Journal of Computational Physics*, Vol. 79, No. 1, pp. 12-49, 1988.

[3] V. Caselles, R. Kimmel and G. Sapiro, "Geodesic Active Contours", *International Journal of Computer Vision*, Vol. 22, No. 1, pp. 61-79, 1997.

[4] S. Kichenassamy, A. Kumar, P. Oliver, A. Tannenbaum and A. Yezzi, "Gradient Flows and Geometric Active Contour Models", *Proceedings of 5th International Conference on Computer Vision*, pp. 810-815, 1995.

[5] C. Li, C. Xu, C. Gui and M.D. Fox, "Level Set Evolution without Re-Initialization: A New Variational Formulation", *Proceedings of IEEE Conference on Computer Vision and Pattern Recognition*, Vol. 1, pp. 430-436, 2005.

[6] C. Li, C. Xu, C. Gui and M.D. Fox, "Distance Regularized Level Set Evolution and Its Application to Image Segmentation", *IEEE Transactions on Image Processing*, Vol. 19, No. 12, pp. 3243-3254, 2010.

[7] R. Ronfard, "Region-Based Strategies for Active Contour Models", *International Journal of Computer Vision*, Vol. 13, pp. 229-251, 1994.

[8] T.F. Chan and L.A. Vese, "Active Contours without Edges", *IEEE Transactions on Image Processing*, Vol. 10, No. 2, pp. 266-277, 2001.

[9] A. Yezzi, A. Tsai and A. Willsky, "A Statistical Approach to Snakes for Bimodal and Trimodal Imagery", *Proceedings of International Conference on Computer Vision*, Vol. 2, pp. 898-903, 1999.

[10] D. Cremers, M. Rousson and R. Deriche, "A Review of Statistical Approaches to Level Set Segmentation: Integrating Color, Texture, Motion, and Shape", *International Journal of Computer Vision*, Vol. 72, No. 2, pp. 195-215, 2007.

[11] S. Lankton and A. Tannenbaum, "Localizing Region-based Active Contours", *IEEE Transactions Image Processing*, Vol. 17, No. 11, pp. 2029-2039, 2008.

[12] S. Lankton, D. Nain, A. Yezzi and A. Tannenbaum, "Hybrid Geodesic Region-based Curve Evolutions for Image Segmentation", *Proceedings of SPIE*, Vol. 6510, pp. 1-8, 2007.

[13] W. Kim and C. Kim, "Active Contours Driven by the Salient Edge Energy Model", *IEEE Transactions on Image Processing*, Vol. 22, No. 4, pp. 1667-1673, 2013.

[14] Zemin Ren, "Adaptive Active Contour Model Driven by Fractional Order Fitting Energy", *Signal Processing*, Vol. 117, pp. 138-150, 2015.

[15] Bo Chen, Shan Huang, Zhengrong Liang, Wensheng Chen, Hanling Lin, Binbin Pan and Marc Pomeroy, "A Fractional Active Contour Model for Medical Image Segmentation", *Proceedings of IEEE Conference on Nuclear Science Symposium and Medical Imaging*, pp. 1-6, 2017.

[16] Ming Gu and Renfang Wang, "Fractional Differentiation-Based Active Contour Model Driven by Local Intensity Fitting Energy", *Mathematical Problems in Engineering*, Vol. 2016, pp. 1-16, 2016.

[17] Bo Chen, Lihong C. Li, Huafeng Wang, Xinzhou Wei, Shan Huang, Wensheng Chen and Zhengrong Liang, "A New Fractional-Order Derivative-based Active Contour Model for Colon Wall Segmentation", *Proceedings of IEEE Conference on Medical Imaging*, pp. 1-7, 2018.

[18] A. Khadidos, V. Sanchez and C. Li, "Weighted Level Set Evolution Based on Local Edge Features for Medical Image Segmentation", *IEEE Transactions on Image Processing*, Vol. 26, No. 4, pp. 1979-1991, 2017.

[19] M.D. Ortigueira and J.A.T. Machado, "What is a Fractional Derivative?", *Journal of Computational Physics*, Vol. 321, pp. 1255-1257, 2016.

[20] R. Hilfer and Y. Luchko, "Desiderata for Fractional Derivatives and Integrals", *Mathematics*, Vol. 7, No. 2, pp. 1-14, 2019.

[21] B. Mathieu, P. Melchior, A. Oustaloup and C.H. Ceyral, "Fractional Differentiation for Edge Detection", *Signal Processing*, Vol. 83, No. 11, pp. 2421-2432, 2003.

[22] Y. Pu and J. Zhou and X. Yuan, "Fractional Differential Mask: A Fractional Differential-Based Approach for Multiscale Texture Enhancement", *IEEE Transactions on Image Processing*, Vol. 19, No. 2, pp. 491-511, 2010.

[23] S. Khanna and V. Chandrasekaran, "Fractional Derivative Filter for Image Contrast Enhancement with Order Prediction", *Proceedings of IET Conference on Image Processing*, pp. 1-6, 2012.

[24] J. Wang, Y. Ye and X. Gao, "Fractional 90 Phase-Shift Filtering based on the Double-Sided Grunwald-Letnikov Differintegrator", *IET Signal Processing*, Vol. 9, No. 4, pp. 328-334, 2015.

[25] J. Li, N. Sang and C. Gao, "Local Fractional Order Derivative Vector Quantization Pattern for Face Recognition", *Proceedings of IEEE Conference on Computer Vision*, pp. 1-13, 2017.

[26] C. Li, C. Kao, J. C. Gore and Z. Ding, "Minimization of Region-Scalable Fitting Energy for Image Segmentation", *IEEE Transactions on Image Processing*, Vol. 17, No. 10, pp. 1940-1949, 2008.

[27] H. Park, T. Schoepflin and Y. Kim, "Active Contour Model with Gradient Directional Information: Directional Snake", *IEEE Transactions on Circuits and Systems for Video Technology*, Vol. 11, No. 2, pp. 252-256, 2001.

[28] R. Kimmel, "Fast Edge Integration", Proceedings of IEEE Conference on Geometric Level Set Methods in Imaging, Vision, and Graphics, pp. 59-77, 2003.

[29] A. Belaid, D. Boukerroui, Y. Maingourd and J. Lerallut, "Phase-Based Level Set Segmentation of Ultrasound Images", *IEEE Transactions on Information Technology in Biomedicine*, Vol. 15, No. 1, pp. 138-147, 2011.

[30] V. Estellers, D. Zosso, X. Bresson and J. Thiran, "Harmonic Active Contours", *IEEE Transactions on Image Processing*, Vol. 23, No. 1, pp. 69-82, 2014.

[31] P. Smereka, "Semi-Implicit Level Set Methods for Curvature and Surface Diffusion Motion", *Journal of Scientific Computing*, Vol. 19, pp. 439-456, 2003.

[32] J. A. Sethian, "Approximation Schemes for Level Set Methods", Cambridge Press, 1996.

[33] S. Osher and R. Fedkiw, "Level Set Methods and Dynamic Implicit Surfaces", Springer, 2003.

[34] Kunal N. Chaudhury and K.R. Ramakrishnan, "Stability and Convergence of the Level Set Method in Computer Vision", *Pattern Recognition Letters*, Vol. 28, pp. 884-893, 2007.

[35] T. Mendona, P.M. Ferreira, J. Marques, A.R.S. Marcal and J. Rozeira, "PH - A Dermoscopic Image Database for Research and Benchmarking", *Proceedings of IEEE International Conference on Engineering in Medicine and Biology Society*, pp. 1-7, 2013.

[36] Ming Ming Cheng, Niloy J. Mitra, Xiaolei Huang, Philip H. S. Torr and Shi-Min Hu, "Global Contrast based Salient Region Detection", *IEEE Transactions in Pattern Analysis and Machine Intelligence*, Vol. 37, No. 3, pp. 569-582, 2015.

[37] Sharon Alpert, Meirav Galun, Ronen Basri and Achi Brandt, "Image Segmentation by Probabilistic Bottom-Up Aggregation and Cue Integration", *Proceedings of IEEE Conference on Computer Vision and Pattern Recognition*, pp. 1-12, 2007.